bioRxiv preprint doi: https://doi.org/10.1101/2021.03.15.435381; this version posted May 10, 2021. The copyright holder for this preprint (which was not certified by peer review) is the author/funder, who has granted bioRxiv a license to display the preprint in perpetuity. It is made available under aCC-BY-NC-ND 4.0 International license.

Changing in the hierarchical organization of local information dynamics during motor decision in the premotor cortex of primates

Giampiero Bardella[1,2], Franco Giarrocco[1,2,], Marta Andujar[1,2], Emiliano Brunamonti[2], Pierpaolo Pani[2], and Stefano Ferraina[2,*]

[1]PhD Program in Behavioral Neuroscience, Sapienza University of Rome, Italy
[2]Department of Physiology and Pharmacology, Sapienza University of Rome, Piazzale Aldo Moro 5, 00185, Rome, Italy
[*]corresponding author(s): Stefano Ferraina (stefano.ferraina@uniroma1.it)

ABSTRACT

Despite recent works have investigated functional and effective cortical networks in animal models, the dynamical information transfer among functional modules underneath cognitive control is still largely unknown. Here, we addressed the issue using Transfer Entropy and graph theory methods on neural activities recorded from a multielectrode array in the dorsal premotor cortex of rhesus monkeys. We focused our analysis on the decision time of a Stop-signal (countermanding) task. When comparing trials with successful inhibition to those with generated movement the local network resulted organized in four classes of modules hierarchically arranged and differently partaking in information transfer. Interestingly, the hierarchical organization of modules changed during the task, being different for generated movements and cancelled ones. Our results suggest that motor decisions are based on a topological re-organization of the premotor functional network.

Introduction

The brain is a complex system formed by different interconnected modules. At the small scale modules are single neurons, at the large scale great-specialized brain areas. In between, at the mesoscale level, modules are aggregates of neurons (populations) of different dimensions (columns; specialized sub-regions; etc). In the last fifty years, neuroscience has tried to describe brain computations by linking neural activities to behaviour. Crucial in this process, at every scale of investigation, is the understanding of how different modules interact and how information is shared and processed among parts. In this context, the neurophysiological approach to brain functions with recording microelectrodes provided invaluable advances, mainly in animal models[1]. Indeed, the high spatial resolution of the method proved to be suitable for linking neurons activity to behaviour, to describe the organization of local microcircuits and, sometimes, of the over standing larger networks[2,3]. Most of these studies referred to the analysis of single unit activity, others focused more on mesoscopic signals as the local field potentials indicating the average synaptic input to the explored area (for a review see[4]) and, to a lesser extent, on signals sampling the average spiking activity of discrete populations[5–7].

Here, aiming to contribute to the understanding of the role of the dorsal premotor (PMd) cortex in arm motor control[8–10] we studied the local spiking activity (SA) derived from a multi-electrode array and implemented a combined information-theory and topological approach based on graph theory to describe how the collective activity of mesoscopically-defined local modules is linked to motor decision-making. Indeed, it has been shown that neurons express more their contribution to complex behavioural functions

bioRxiv preprint doi: https://doi.org/10.1101/2021.03.15.435381; this version posted May 10, 2021. The copyright holder for this preprint (which was not certified by peer review) is the author/funder, who has granted bioRxiv a license to display the preprint in perpetuity. It is made available under aCC-BY-NC-ND 4.0 International license.

either when observed as coordinated functional ensembles[11–19] or described as common responses to the input they receive (e.g., the visual stimulus orientation columns[20]). A paradigmatic example of functional interaction is the interplay between fixation and movement neurons in the epochs preceding saccade generation[13,14]. In the present work we inspected how information is managed among local modules in PMd and how this network is arranged during either movement execution or cancellation. How different neuronal actors contribute to motor decisions is in fact still largely discussed, especially for brain centres involved in reaching control[10,21]. We observed that motor decision-making in PMd is linked to modules of information management that segregate into different classes hierarchically organized and change in relation to the behavioural outcome. Moreover, with graph theory tools, we demonstrated that the PMd network undergo different configurations depending on the behavioural decision. Indeed, during movement generation, compared to movement inhibition, information transmission among modules was more efficient requiring fewer steps. This demonstrates that information among population of neurons is processed differently during the two motor behaviours explored and suggests a new perspective on the view of how the local computation evolves in motor areas during motor decisions.

Results

We investigated, at the mesoscopic scale, the information transfer and functional directed connectivity patterns among discrete populations of neurons during the motor decision phases of arm movements. To this aim we extracted a measure of the local SA from each electrode of a microelectrode array (up to 96 channels) in the PMd of two male Rhesus monkeys while they performed a countermanding reaching task. This task (Fig. 1) required either to move the arm toward a peripheral target (Go trials; 75%) or to cancel the movement in case of appearance of a Stop signal (Stop trials; 25%). The two types of trials were randomly presented. During **Go trials**, after the disappearance of the central target (Go signal) the monkeys were instructed to reach the peripheral target to obtain the reward. In **Stop trials**, after the Go signal, the central target reappeared (Stop signal) after a variable delay, called SSD (Stop signal delay). In these trials the monkeys were required to refrain from moving to earn the reward (correct Stop trials). If the monkey were unable to stop, the trials were classified as wrong Stop trials, and no reward was provided. Because the SSDs were varied according to a staircase procedure based on the performance, correct Stop trials constituted approximately 50% of Stop trials (see Table 1). This task allows to estimate behaviorally the time window during which the decision to move (or to refrain) is taken. This time window is commonly referred as the Stop signal reaction time (SSRT; see Table 1 for the values measured in the present study). For the analysis of the SA, among animals and recording sessions, we used a fixed epoch duration (T = 400 ms). This epoch (see Figure 1; grey bar) was built to include the estimated duration of the SSRT for each recording session and part of the last portion of the SSD (see figure 2 and Materials and Methods for details).

Local spiking activities can be grouped in classes providing different contribution to the network information dynamics

We investigated a total of 21 recording sessions (12 for monkey P and 9 for monkey C). For each session we derived a measure of the SA (see Materials and Methods) from all neurons firing in close proximity of the tip of each electrode. From now on we refer for simplicity to these discrete neuronal populations as modules.

Fig 2 shows, for one example session, the SAs of both Go trials (green traces) and Stop trials (red traces) in the above referred epoch T and for each of the modules recorded. Most modules display a clear difference of SAs between correct Stop trials and Go trials after the Stop signal (vertical red line), i.e.,

bioRxiv preprint doi: https://doi.org/10.1101/2021.03.15.435381; this version posted May 10, 2021. The copyright holder for this preprint (which was not certified by peer review) is the author/funder, who has granted bioRxiv a license to display the preprint in perpetuity. It is made available under aCC-BY-NC-ND 4.0 International license.

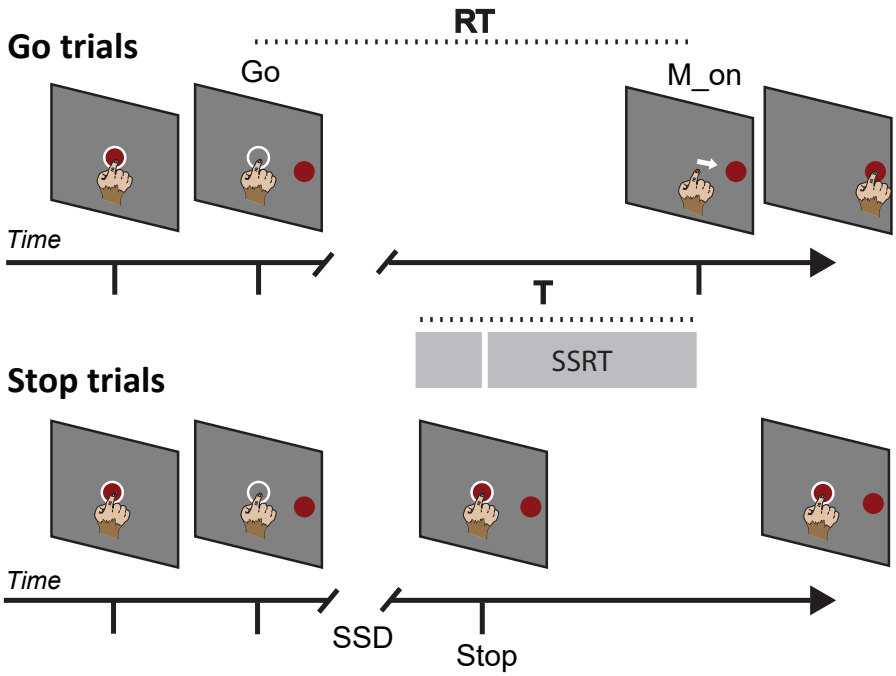

Figure 1. Sequence of behavioural events characterizing the task. Go and Stop trials were randomly intermixed during each session. The epoch (T) of neural analysis is shown as a grey bar. For Go trials, the SSRT marks the time, before movement execution, that would have corresponded to the presentation of the Stop signal. For correct Stop trials SSRT marks the time, after the Stop signal presentation, that would have corresponded to the movement execution. RT, reaction time; SSD, Stop signal delay; SSRT, Stop signal reaction time. White circles are feedbacks for the touch provided to the animals. Go: time of Go signal appearance; Stop: time of Stop signal appearance.

during the session-specific SSRT, reflecting the active participation of PMd in the decision to generate or inhibit reaching movements. Several features are observable. For example, the time of divergence between the two activities for the different modules was highly variable. Moreover, in some cases (e.g., modules 25, 43, 65, and 67) the observed pattern was completely opposite (more intense activity in Stop trials than in Go trials). A similar overall picture was evident in all recorded sessions. In short, the various modules seem to contribute to the control exerted by PMd on the movement to be performed in a very heterogeneous way. However, from these considerations nothing could be inferred about the information transfer and the functional relationship between different modules.

To study information transfer between the network modules we used Transfer Entropy (TE), a well-established model-free information theoretic method[22]. In a given epoch TE can detect asymmetric information flows among the modules, and hence it allows defining modules acting as drivers (or sources) or targets of information transfer (see Materials and Methods for further details). To evaluate whether the different behavioural conditions of the task were characterized by different local information dynamics we computed TE between trial-averaged time series (i.e., in the epoch T) of SA separately for Go and correct Stop trials. We found that some of the modules were drivers in both Go and Stop conditions (**Common_drivers**); others were drivers in one behavioural condition only (**Go_drivers** and **Stop_drivers**); others were never drivers and just targets of information flow (**Targets**) (see Table 2 for the average distribution among sessions; see Materials and methods for further details). The presence of

bioRxiv preprint doi: https://doi.org/10.1101/2021.03.15.435381; this version posted May 10, 2021. The copyright holder for this preprint (which was not certified by peer review) is the author/funder, who has granted bioRxiv a license to display the preprint in perpetuity. It is made available under aCC-BY-NC-ND 4.0 International license.

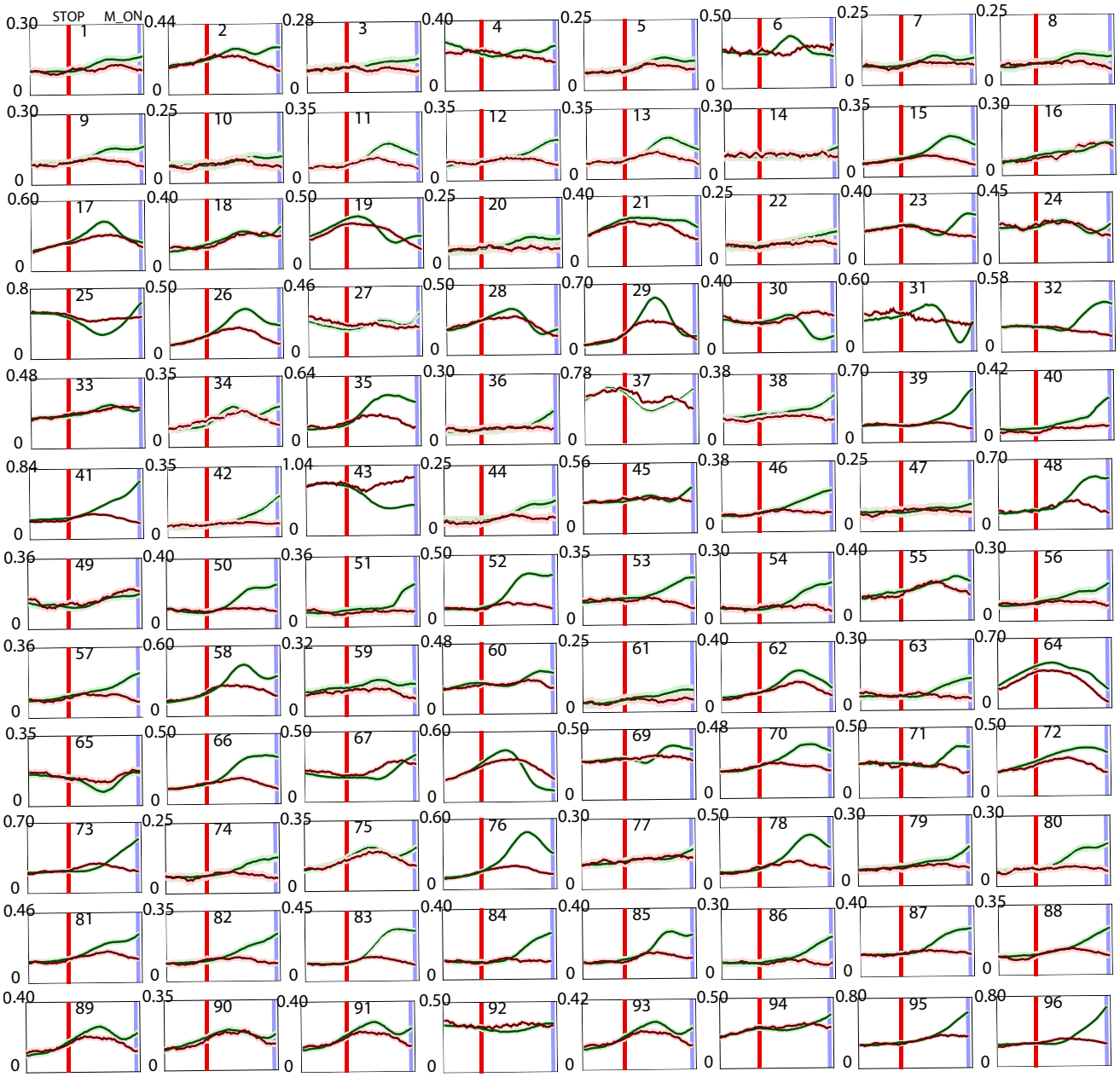

Figure 2. Neuronal SAs in the two behavioural conditions for all modules of a typical recording session. Green traces show the average activity during Go trials aligned to Movement onset (blue vertical line). Red traces show the average activity during correct Stop trials aligned to the Stop signal presentation (red vertical line). The epoch between the Stop signal and the movement onset is the session SSRT.

bioRxiv preprint doi: https://doi.org/10.1101/2021.03.15.435381; this version posted May 10, 2021. The copyright holder for this preprint (which was not certified by peer review) is the author/funder, who has granted bioRxiv a license to display the preprint in perpetuity. It is made available under aCC-BY-NC-ND 4.0 International license.

Behavioural Results						
Monkey P						
S	$\overline{RT_{Go}}$	$\overline{RT_{Wr}}$	$\overline{SSD}$	***SSRT***	$\mathbf{P_{inhibit}}$	***p-value***
1	590 ms	559 ms	273 ms	317 ms	0.52	$p < 0.05$
2	584 ms	564 ms	277 ms	307 ms	0.50	$p < 0.05$
3	575 ms	503 ms	293 ms	282 ms	0.69	$p < 0.05$
4	618 ms	592 ms	335 ms	283 ms	0.52	$p < 0.01$
5	868 ms	549 ms	675 ms	193 ms	0.58	$p < 0.01$
6	572 ms	540 ms	293 ms	279 ms	0.50	$p < 0.05$
7	643 ms	622 ms	382 ms	261 ms	0.51	$p < 0.05$
8	600 ms	568 ms	340 ms	260 ms	0.48	$p < 0.01$
9	656 ms	641 ms	445 ms	211 ms	0.37	$p < 0.01$
10	788 ms	753 ms	528 ms	260 ms	0.54	$p < 0.01$
11	674 ms	619 ms	418 ms	256 ms	0.56	$p < 0.01$
12	765 ms	721 ms	504 ms	261 ms	0.51	$p < 0.01$
Monkey C						
1	598 ms	523 ms	322 ms	276 ms	0.57	$p < 0.01$
2	539 ms	460 ms	382 ms	157 ms	0.65	$p < 0.05$
3	561 ms	522 ms	318 ms	243 ms	0.58	$p < 0.01$
4	673 ms	625 ms	424 ms	249 ms	0.60	$p < 0.05$
5	636 ms	608 ms	396 ms	240 ms	0.55	$p < 0.05$
6	575 ms	533 ms	292 ms	283 ms	0.42	$p < 0.01$
7	667 ms	620 ms	383 ms	284 ms	0.60	$p < 0.05$
8	688 ms	672 ms	413 ms	275 ms	0.43	$p < 0.05$
9	688 ms	657 ms	402 ms	286 ms	0.60	$p < 0.01$

Table 1. Behavioural results. S, index of the recording session. $\overline{RT_{Go}}$, mean reaction time of Go trials. $\overline{RT_{Wr}}$, mean reaction time of wrong Stop trials. $\overline{SSD}$, mean SSD of Stop trials. $SSRT$, Stop signal reaction time. $P_{inhibit}$, inhibition probability. The *p-values* result from the independence (Kolmogorov-Smirnov test between RT_{Go} and RT_{Wr} distributions).

different classes straightforwardly showed that the intrinsic composition of the PMd information network is heterogeneous, with some of the modules operating as drivers only in relation to a specific behavioral outcome (moving vs withholding). This hinted that the network configuration underlying information transmission changes according to the decision leading to a specific behavioural output.

Neuronal activity classes are hierarchically organized

To better understand the role of the identified classes (i.e, Common_drivers, Go_drivers, Stop_drivers and Targets) in the PMd network we investigated the topology of information transmission for each recording session and behavioural condition. In this framework, each entry of the TE matrix is interpreted as a node of the network and each link (or connection) as the information exchanged between nodes (see Materials and methods for further details). To describe the topology of information transmissions we resorted to different graph-based measures.

bioRxiv preprint doi: https://doi.org/10.1101/2021.03.15.435381; this version posted May 10, 2021. The copyright holder for this preprint (which was not certified by peer review) is the author/funder, who has granted bioRxiv a license to display the preprint in perpetuity. It is made available under aCC-BY-NC-ND 4.0 International license.

Classes Composition	
Monkey P	$N = 96$
Class	$\boldsymbol{\mu \pm SD}$
Go_drivers	6.46 ± 2.90
Stop_drivers	13.71 ± 3.22
Common_drivers	8.62 ± 3.60
Targets	67.20 ± 4.88
Monkey C	$N = 79$
Class	$\boldsymbol{\mu \pm SD}$
Go_drivers	6.78 ± 3.93
Stop_drivers	9.56 ± 3.78
Common_drivers	7.00 ± 2.06
Targets	55.70 ± 5.29

Table 2. Classes composition. For each monkey the composition of classes averaged over recording sessions is reported. Composition is expressed as the average number of nodes (μ) belonging to each class. SD, standard deviation. N, the number of channels available.

We first computed the **vertex degree** (VD), i.e. the number of connections per module. A high value of the VD indicates that the module is functionally connected with many others. The opposite holds for a low value of VD. Thanks to the asymmetry of TE, which defines drivers and targets, for each module it is possible to distinguish between the information directed towards other modules (VD_{out}) and the information incoming from other modules (VD_{in}). We examined the VD_{out} and the VD_{in} distributions for each recording session of both monkeys and we observed that only the VD_{out} distributions were fat-tailed (see supplementary Figure S1). The high values of VD_{out} associated to the tails indicate the presence of modules with a number of outwards connections that greatly exceed the average value (see Materials and Methods). These modules are commonly defined as network hubs[23]. As a consequence, we focused only on the VD_{out} distribution details. The direction of information flow detected by TE along with the VD values, allow defining a hierarchy of information transmission among modules. Indeed, according to the TE-based definition of drivers and targets, the past of a driver gives statistical significant contribution to the prediction of the present state of a target. This puts the drivers hierarchically above the targets. Moreover, the existence of networks hubs means that a few modules determine the state of many others and hence the global configuration of the network. Fig 3 shows the topology of the PMd network in both behavioural conditions for data in Figure 2 (see also Figure S2). Each module is assigned to a class as previously obtained from the analysis of the TE distributions and coloured accordingly. The arrow for each connection indicates the direction (in/out) for the information path; thus the number of outgoing connections of each module reflect its VD_{out} value, i.e. the number of modules on which it acts as a driver. In Go trials (left) the topology documented a more centralized (in terms of VD_{out}) organization compared to the Stop trials (right), confirming previous observations[18]. With the insights provided by the TE analysis, the emerging picture is of a network changing not only in the overall organization but also in the role of the components. To this extent, Fig 3 shows that Stop_drivers emerge as important nodes in information spreading in Stop trials only.

Figure 4 (top panels) shows, for all sessions, that the Common_drivers exhibited the highest values of

bioRxiv preprint doi: https://doi.org/10.1101/2021.03.15.435381; this version posted May 10, 2021. The copyright holder for this preprint (which was not certified by peer review) is the author/funder, who has granted bioRxiv a license to display the preprint in perpetuity. It is made available under aCC-BY-NC-ND 4.0 International license.

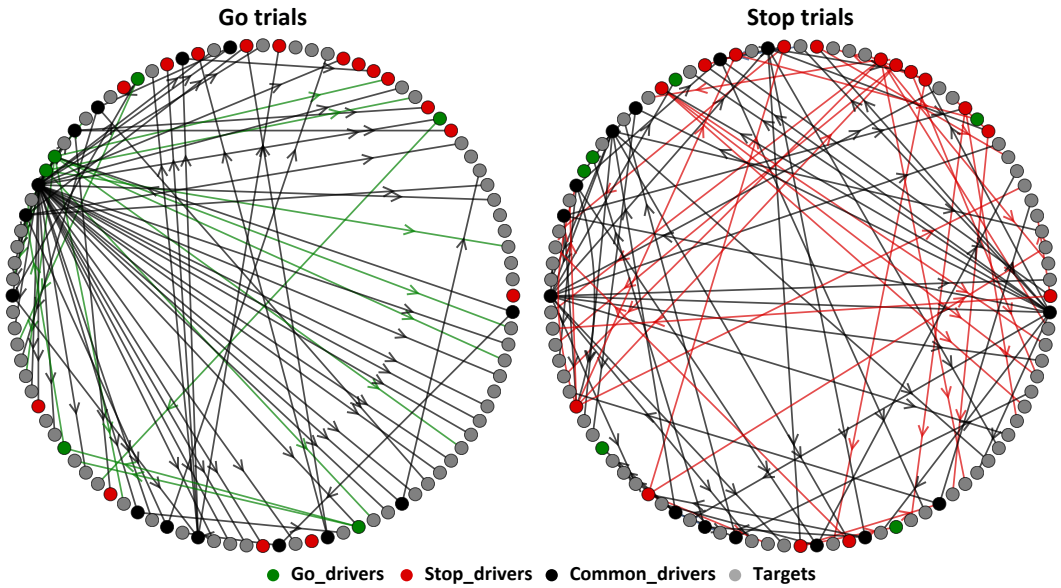

Figure 3. Information network of Go and Stop trials for data in Figure 2. Each node and the respective connections are colour coded accordingly to the corresponding class (see legend in the lower part of the figure). Nodes with an high number of outgoing connections are the information-spreaders hubs (see text for details).The coordinates of each node on the circle are preserved in both plots.

VD_{out} (See Table 3 for the corresponding statistics) compared to other classes in both Go and correct Stop trials, thus resulting as the principal information-spreaders hubs across different behavioural conditions. Therefore, the Common_drivers are located at the highest hierarchical level in the network as they regulate information transfer whatever decision, moving or stopping, is taken (see also next paragraph). Conversely, the Go_drivers and the Stop_drivers displayed a different role (different VD_{out} values) in Go and Stop trials, suggesting that the hierarchical organization of the network changes in relation to the motor decision process. Indeed, the Stop_drivers are never hubs in Go trials and the Go_drivers are never hubs in Stop trials.

As a further measure of the organization of the PMd network we used **betweenness centrality**[24,25] (BC). BC quantifies the influence that a given node has over the flow of information between other nodes. Therefore, it gives a measure of how a node controls communications in a network. BC is computed as the fraction of paths between all nodes in the network that pass through a given node (see Materials and Methods). Since we are dealing with an information network, we used BC to quantify the capability of each node to mediate and route the information traffic. An high BC value indicates that a node lies on a considerable fraction of paths between other nodes and therefore it strongly mediates the information flow in the network. Hence, nodes with high BC values are topological central nodes. As reported in Fig 4 (bottom panel) and in Table 3, we found higher BC values during correct Stop trials compared to Go trials meaning that during correct Stop trials information traverses an higher number of paths. This implies that a shift toward a less direct (and hence less centralized in terms of VD_{out}) communication between nodes occurs only during Stop trials, where information is detoured through more paths resulting in a more distributed and widespread transmission scheme. An intuition can be gained by noticing the arrangement of the networks during correct Stop trials in which information transmission appears to more "scattered", with the connections between nodes arranged in a more distributed way rather than radially outgoing from the high-degree nodes as in Go trials (see Figure 3). Analogously to what found during the

bioRxiv preprint doi: https://doi.org/10.1101/2021.03.15.435381; this version posted May 10, 2021. The copyright holder for this preprint (which was not certified by peer review) is the author/funder, who has granted bioRxiv a license to display the preprint in perpetuity. It is made available under aCC-BY-NC-ND 4.0 International license.

analysis of VD_{out}, the Go_drivers and the Stop_drivers (green and red dots in Fig 4) displayed a different role (different BC values) in Go and correct Stop trials respectively, confirming the specificity of these classes in relation to the behavioural conditions. The values of BC found for the Common_drivers (black dots in 4) during both behavioural conditions corroborate what was found via the VD_{out} analysis: in the PMd information network they manage and distribute the information flow. Moreover, during movement inhibition the actors that collaborate the most with the Common_drivers in rerouting and reverberating communications are the Stop_drivers. It is important to highlight (see Figure 4 and Figure S2) that the Common_drivers are also modulated by the task condition. In fact, those emerging as hubs are often different in Go and Stop trials.

To have a compact view of the overall differences between the VD_{out} and the BC measures across behavioural conditions, we computed a summarising index for both topological measures named **centralization index** C[24,25]. C is the total average difference between the highest value of the centrality measure used (VD_{out} and BC in our case) and the values assumed by all the other nodes. High values of C indicate that nodes with high centralities with respect to the other nodes in the network exist. C is an easy and intuitive way to compare the overall organization of networks in terms of centrality measures (see Materials and Methods). We computed C for both centrality measures for each recording session and then we averaged over sessions. Panel A of Figure 5 reports the average centralization indexes compared between behavioural conditions for both animals (results from each sessions are reported in panel A of supplementary figure S3). As expected, C of VD_{out} (C_{vd}) decreases from Go to correct Stop trials while the opposite holds for C of BC (C_{bc}). This confirms, at the overall level, how information processing is based on different underlying topologies during the two behavioural conditions.

We then calculated the **total information** TE_{total} processed during Go trials and correct Stop trials (Figure 5, panel B and supplementary figure S3 panel B). We found that during correct Stop trials less information was processed compared to Go trials. This means that the overall changes in the topological arrangement of the the PMd network correspond to overall changes in the amount of information exchanged. More specifically, the decrease of VD_{out} and the increase of BC during correct Stop trials are accompanied by a reduction in the total amount of information elaborated.

To sum up, we demonstrated that the TE-defined classes are hierarchically organized in PMd during movement planning and suppression and that information is processed differently during correct Stop trials compared to Go trials. Results revealed the Common_drivers as the most topological central nodes in the network with the Go_drivers and the Stop_drivers playing a crucial supporting role in the processing of information during movement planning and inhibition respectively.

Different interactions among neuronal classes characterize behavioural conditions

To summarize the interactions among classes we computed the average amount of information exchanged between the four classes during both behavioural conditions. To this end, we constructed a 4x4 matrix of the interaction index I (see Materials and Methods). We then represented the **matrix I** as a network in which each node is now a class. This makes possible to have a compact picture of the differences between Go and correct Stop trials in terms of interactions between classes. We calculated I for both behavioural conditions of each recording session and we then averaged over sessions; results are schematically shown in Figure 6 (see Table 4 for details). The Common_drivers were confirmed to be part of the high order class in the network since they transmit to other classes without receiving. Indeed, even when the Go_drivers and the Stop_drivers emit information on their own, they receive from the Common_drivers. This means that the first ones are hierarchically located at a lower level. Moreover, the extent of communication of the Common_drivers with the Targets is significantly greater than that of the Go_drivers and the Stop_drivers (see Table 4). This implies that the Common_drivers determine the global state of the

bioRxiv preprint doi: https://doi.org/10.1101/2021.03.15.435381; this version posted May 10, 2021. The copyright holder for this preprint (which was not certified by peer review) is the author/funder, who has granted bioRxiv a license to display the preprint in perpetuity. It is made available under aCC-BY-NC-ND 4.0 International license.

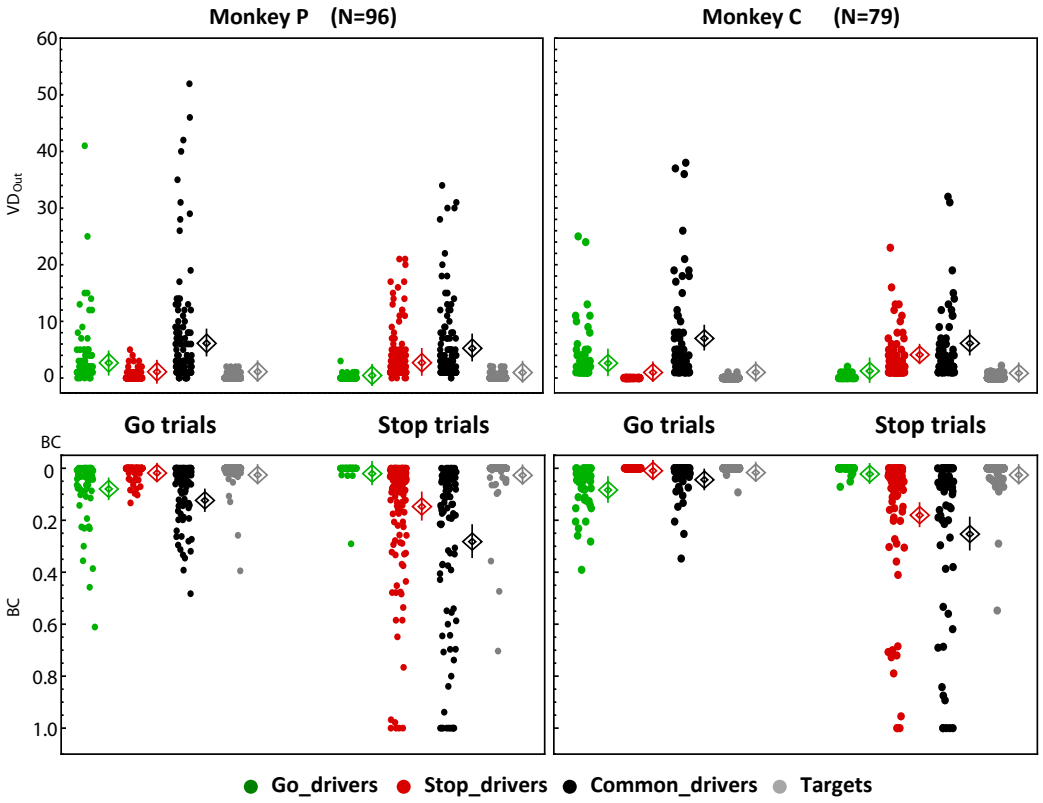

Figure 4. Measures for topology of information transmission. **Top panels**: VD_{out} values compared across behavioural conditions for all recording sessions. The Common class (black points) shows the highest values of VD_{out} compared to other classes in both behavioural conditions (for both monkeys, all adjusted p-values $Qs < 0.01$). Go_drivers and Stop_drivers show the second highest VD_{out} values during Go (for both monkeys all $Qs < 0.01$) and correct Stop (for both monkeys all $Qs < 0.01$) trials respectively. **Lower panels**: BC values compared across behavioural conditions for all recording sessions (here scaled for simplicity to the maximum value of each session so to have values in the range [0,1]). Go_drivers and Stop_drivers classes have, together with the Common, the highest values of BC during Go and correct Stop trials respectively (for both monkeys all $Qs < 0.01$). The Stop_driver class is the one with the greatest increase ($\Delta_{Stop-Go}$) in BC passing from Go to correct Stop trials (for both monkeys all $Qs < 0.01$). Colours reflect the neuronal classes as in Figure 4. Means and standard errors are indicated by the diamonds and related lines. Statistics is based on the adjusted p-value (Q) obtained from Kolmogorov Smirnoff tests and false discovery rate (FDR) correction. See Table 3 for the details.

network with the Go_drivers and the Stop_drivers playing a supporting role. It is worth noticing that the specificity of the Go_drivers and the Stop_drivers is confirmed by the direction of their interactions during behavioural conditions. Indeed, during Go trials the Go_drivers transmit to the Stop_drivers helping the Common_drivers in the control while the opposite happens during correct Stop trials. The amount of information that the Common_drivers distribute in the network diminishes from Go to correct Stop trials. This complements and helps to better understand what said in the previous section: the patterns of information transfer change from Go to correct Stop trials, with the network undergoing a less direct configuration during the latter due to an increased number of paths between the nodes. Network interactions are consistent across recording sessions for both monkeys (see Table 4). Common_drivers are

bioRxiv preprint doi: https://doi.org/10.1101/2021.03.15.435381; this version posted May 10, 2021. The copyright holder for this preprint (which was not certified by peer review) is the author/funder, who has granted bioRxiv a license to display the preprint in perpetuity. It is made available under aCC-BY-NC-ND 4.0 International license.

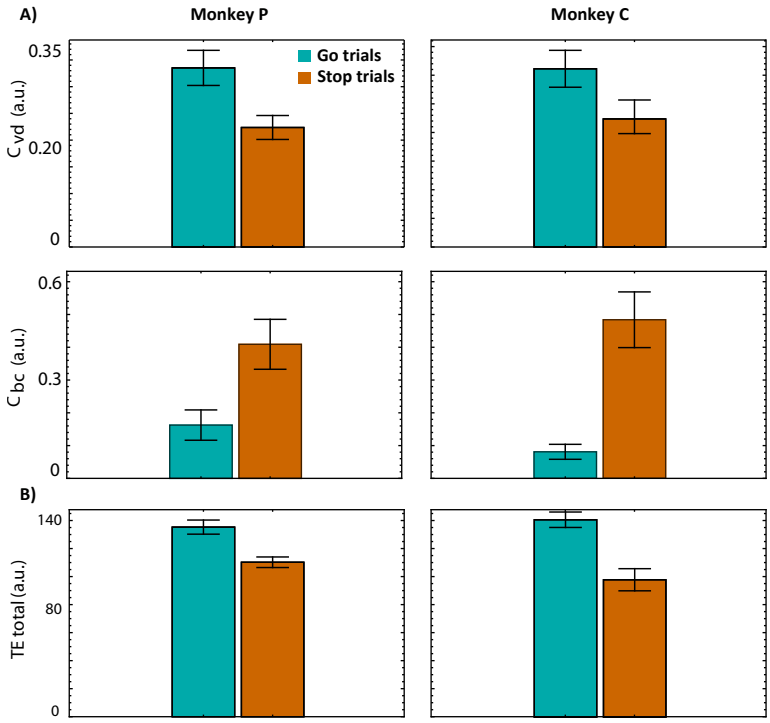

Figure 5. Overall network comparison between behavioural conditions. Panel A: The overall centralization index C for both VD_{out} (C_{vd}) and BC (C_{bc}) measures averaged over recording sessions and compared between behavioural conditions for both monkeys. **Panel B:** Total information processed averaged over recording sessions compared between behavioural conditions. Cyan: Go trials. Orange: correct Stop trials. Error bars are given by the standard error of the mean.

always hierarchically above the other classes and orchestrate communication: they transmit information to other classes in both behavioural conditions without receiving information from the other classes of the analysed PMd network. Moreover, during Go trials, the Go_drivers participate transmitting to the Targets as the Stop_drivers do during correct Stop trials.

Discussion

In this work we investigated the patterns of information transfer in a localized cortical network (the PMd) directly involved in movement decision-making. We used a combined Transfer Entropy and graph theory-based approach to analyse simultaneously recorded SAs (from up to 96 channels). Our results contribute to move forward the knowledge on the neural basis of motor control at different levels.

A topological approach to the organization and spreading of local information in a motor decision task

The first level of advancement is methodological: we employed a graph theory approach combined with information theoretic measures (specifically Transfer Entropy) to investigate neuronal interactions underlying motor control. Although TE is growing in popularity in modern neuroscience its application to invasive electrophysiological data has been so far very limited and restricted mostly to either single neurons or in vitro[26–28] and in silico studies[29]. Shimono and Beggs[26] used it at the single neuron level to investigate the structure at different scale of rodent somatosensory cortex[26,30]. Timme and colleagues[31]

bioRxiv preprint doi: https://doi.org/10.1101/2021.03.15.435381; this version posted May 10, 2021. The copyright holder for this preprint (which was not certified by peer review) is the author/funder, who has granted bioRxiv a license to display the preprint in perpetuity. It is made available under aCC-BY-NC-ND 4.0 International license.

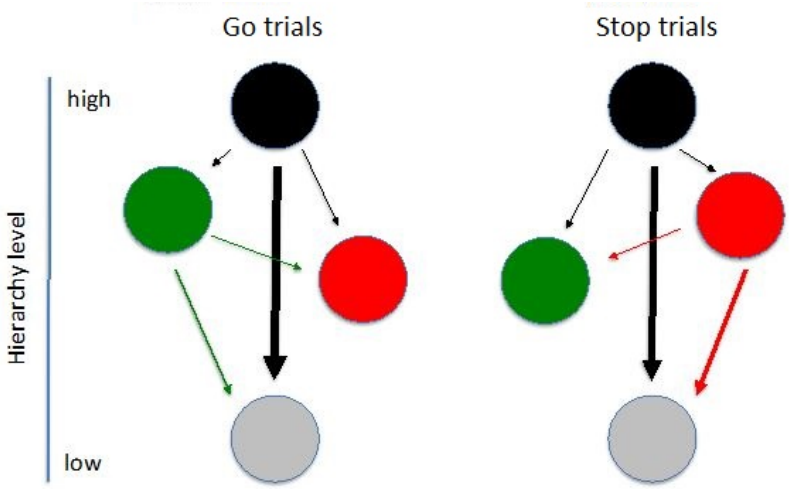

Figure 6. Network representation of interactions between classes in the two behavioural conditions: Colours codes for the classes are the same of the previous figures. The size of the arrows provide a measure of the average value of I (see text).

recorded the activity of hundreds of neurons in cortico-hippocampal slice cultures and used TE to study the information transfer changes therein. An early contributions to this research topic is from Gerhard et al[32] that inspected the topology of spike trains recordings from the visual system of a rhesus monkey during a fixation task. However, the authors used a different approach to measure directed connectivity (the use of TE on invasive electrophysiological data from the visual system is also attributable to Besserve and collegues[33] which however did not resort to graph theory techniques). Another contribution comes from the work of Honey[34], that investigated a large-scale interregional anatomical network of the macaque cortex trough Transfer Entropy. An attempt to study voluntary action control through analysis of directed connectivity was made by Jahfari and colleagues[35] but on human MRI data. Hence, to the best of our knowledge, this report is one of the very few studies that uses graph theory to analyse the information transfer network of a specific cortical area at the mesoscale level in vivo and during a behavioural task. The level of description here obtained is more detailed compared to previous works. Indeed, we were able to specify how the decision on whether to move or to stop is implemented in PMd at the population level and who are the (key) players that manage information transmission. Notably, in our framework neither any a priori assumption nor a specific neural modelling technique was needed. Our completely data-driven approach, in addition to complement the most recent models for motor generation and suppression[36,37], permits to overcome their main limitation which resides in the requirement of many biophysical parameters to be tweaked and tuned before fitting with acceptable accuracy the experimental data. Although is still not largely used in behavioural neurophysiological studies at the small and mesoscale, a graph theory-based conceptualization of neural interactions, united with information theoretic measures, can be very profitable also compared to other common approaches relying on the analysis of covariance between neurons or mesoscopic signals[7,38–41] and should be exploited more. In fact, these methods are not straightforward in distinguishing the specific contributions of single neurons (or discrete populations of neurons) to the topology of network dynamics, which is indeed the strength of our strategy. On one hand, this range of methods allows for a fine temporal description of neural variability but on the other, due to their nature, are neither capable to describe the information flow between neuronal actors nor to provide quantitative insights on the topology of network connections and their hierarchical organization. Without this spectrum of details the computational strategy underlying motor control (and neural circuitry

bioRxiv preprint doi: https://doi.org/10.1101/2021.03.15.435381; this version posted May 10, 2021. The copyright holder for this preprint (which was not certified by peer review) is the author/funder, who has granted bioRxiv a license to display the preprint in perpetuity. It is made available under aCC-BY-NC-ND 4.0 International license.

computation in general) would be yet elusive. Recently, some authors have started to follow the joint information theory-complex networks approach but for now, to the best of our knowledge, only on cortico-hippocampal[31], somatosensory cortex slice cultures[26] and during anesthesia[42]. It is known that to fully understand the neural mechanisms behind motor control future research should focus on cortico-cortical and cortico-subcortical interactions through massive simultaneous recordings. In this scenario, a topological information-based approach would be unquestionably necessary to gain an overall view and elicit detailed insights.

A race with more than two horses is in act in PMd when movements are successfully suppressed

The second level of advancement concerns the novelty of our results compared to other studies, especially those that focused on the possible interaction among different classes of neurons during motor decision. We found, in the characterized PMd network, that neuronal activities could be organized around four different classes and that they actively participate, even with different roles (i.e., through different topological attributes), both in movements execution and cancellation. This constitutes a step forward in the conceptualization of the neural processes at the base of movement generation since all the widely accepted models for inhibitory control of movements[36,37,43–46] are deduced from the analysis of data from single electrodes recordings and are based on the interaction of only two modules (or class of neurons) often reported as Go and Stop units. We instead demonstrated that information is hierarchically transferred between more than two actors with the Common class nodes acting as network hubs. This reflects the existence of an intrinsic high-order complexity in functional communications and organization at the population level, even in small portions of the cortex, during behavioural control regardless of which the nature of neurons in each class might be (e.g., excitatory or inhibitory neurons). Indeed, based only on the information emitted by each local module, we managed to isolate both condition-specific and non specific neuronal classes. It is worth stressing that we drew our conclusion on the heterogeneity of neuronal classes in a completely data-driven and model-free fashion, and this strengthens the results. Additionally, we showed the details of how this transfer occurs at the population level and to what extent it is linked to different behavioural outcomes. Our picture integrates the current view because besides specific classes involved in the generation (Go_drivers) and inhibition (Stop_drivers) of movements, it establishes the existence of a high order class (Common_drivers) not proposed in other works. This highlights, for the first time at the mesoscale resolution, the existence of a fine-grained organization of neural assemblies at the population level that handle intra-area information flow. It is worth pointing out that usual methods of studying neural activity profiles are not sufficient to infer all aspects of such architecture. The Common_drivers are higher in hierarchy with respect to the others for two reasons. The first is because they transmit information to the whole network without receiving from inside the same network. Indeed, from the information theoretic point of view, this means that the state of the other classes can be better predicted by the state of the Common compared to that of the other classes. Thus, the state of the whole local network depends on the state of the Common_drivers. The second one is topological, being the Common_drivers the most widespread hubs across behavioural conditions. The found subdivision in classes, the presence of hubs and topological central nodes deputed to the rerouting of communications reveal that the cortical information dynamics behind motor control is extremely rich and cannot be entirely explained by the current proposed models. The found topology also implies that the presence of high-degree nodes is a constituent feature of neural processing in a cortical network directly involved in cognitive control, as is the PMd. This is consistent with our previous study[18] in which we showed how the functional PMd network organization differs between movement generation and inhibition in terms of hierarchy and centrality of nodes. It is also in agreement with other works that found

bioRxiv preprint doi: https://doi.org/10.1101/2021.03.15.435381; this version posted May 10, 2021. The copyright holder for this preprint (which was not certified by peer review) is the author/funder, who has granted bioRxiv a license to display the preprint in perpetuity. It is made available under aCC-BY-NC-ND 4.0 International license.

fat-tailed degree distributions in silico[47], in cortical and hippocampal in vitro networks[26,48–51], in vivo[52] and anatomical structural networks[34]. We found that the arrangement of the PMd information network depends on the behavioural condition, passing from a centralized state during movement planning to a different one during movement inhibition characterized by high values of Betweenness Centrality and a minor transfer of information.

We interpret the reorganization as the execution in the local network of a command originating from other regions. Indeed, as known, the PMd is part of a larger network surbserving motor control based on frontal, parietal, subcortical and spinal structures. It is reasonable to think that during Go trials the hubs serve to convey the command to move to other (and possibly anatomically lower) cortical, subcortical, and spinal circuits that will eventually promote muscle activation. In this picture, the state observed during correct Stop trials could reflect the PMd collective reaction to the incoming inhibitory thalamic input that prevents the execution of the programmed movement. Therefore, the volition to inhibit would be locally implemented as 'the attenuation of the movement state', which seems convenient ad easy to implement at the network level by detouring information flow through an higher number of paths between nodes and decreasing the amount of information involved. Future studies will be necessary to investigate to whom the hubs project to. One weakness of this study is that we cannot account for the information dynamic between PMd and other structures of the reaching network. Therefore, additional research will be needed to unambiguously clarify these interactions. Lo et al.[37] also introduced a certain degree of hierarchical organization in the form of a top-down control regulating the activation of the Go and Stop units. However, as also stated in Schall et al.[45], the control unit embodied in their model resembled an external homunculs endowed with the ability to tune the parameters to appropriately obtain the desired results. This marks a considerable difference with our report, in which, since our approach is completely data-driven, we did not need to adjust any external modelling unit to obtain the results. Conversely, we used it conceptually to contextualize our results in a wider circuitry frame. Lastly, our findings clearly show that hierarchical control is not only external but is also implemented locally by a specific neuronal class (the Common_drivers) over the others. Throughout the years, much evidence has been brought to support the idea that the brain is hierarchically organized both globally and locally on a spatial[18,53–64] (for a detailed review see Hilgetag et al., 2020[65]) and temporal scale[66–71]. As far as we know, this is the first work that deeply investigates the local hierarchy of a single cortical area known to have a crucial role in the motor system. These conclusions suggest that the collective network organization found in this work represents the neural implementation for the voluntary motor control at the PMd level.

Materials and methods

Subjects

Two male rhesus macaque monkeys (Macaca mulatta, Monkeys P and C), weighing 9 and 9.5 kg, respectively, were used. Animal care, housing, surgical procedures and experiments conformed to European (Directive 86/609/ECC and 2010/63/UE) and Italian (D.L. 116/92 and D.L. 26/2014) laws and were approved by the Italian Ministry of Health. Monkeys were pair-housed with cage enrichment. They were fed daily with standard primate chow that was supplemented with nuts and fresh fruits if necessary. During recording days, the monkeys received their daily water supply during the experiments.

Apparatus and task

The monkeys were seated in front of a black isoluminant background ($< 0.1cd/m2$) of a 17-inch touchscreen monitor (LCD, 800 x 600 resolution), inside a darkened, acoustic-insulated room. A non-commercial software package, CORTEX (http://www.nimh.gov.it), was used to control the presentation

bioRxiv preprint doi: https://doi.org/10.1101/2021.03.15.435381; this version posted May 10, 2021. The copyright holder for this preprint (which was not certified by peer review) is the author/funder, who has granted bioRxiv a license to display the preprint in perpetuity. It is made available under aCC-BY-NC-ND 4.0 International license.

of the stimuli and the behavioural responses. Fig. 1 shows the scheme of the general task: a reaching countermanding task[72]. Each trial started with the appearance of a central target (CT) (red circle, diameter 1.9 cm). The monkeys had to reach and hold the CT. After a variable holding time (400–900 ms, 100-ms increments) a peripheral target (PT) (red circle, diameter 1.9 cm) appeared randomly in one of two possible locations (right/left) and the CT disappeared (Go signal). In Go trials, after the Go signal the subjects had to reach and hold the PT for a variable time (400-800 ms, 100*ms* increments) to receive juice. Reaction times (RTs) were defined as the time between the presentation of the Go signal and the onset of the hand movement. In Stop trials, the sequence of events was the same until the Go signal. Then, after a variable delay (Stop signal delay, SSD), the CT reappeared (Stop signal) and the monkeys had to hold the CT until the end of the trial (800–1000 ms) to receive the reward (correct Stop trial). Conversely, removing the hand after the Stop signal constituted a wrong response (wrong Stop trial). The same amount of juice was delivered for correct Stop and correct Go trials. The intertrial interval was set to 800 ms. Stop trials represented the 25% of all trials in each recording session. To establish the duration of the SSDs, a staircase tracking procedure was employed. If the monkey succeeded in withholding the response, the SSD increased by one step (100 ms) in the subsequent Stop signal trial. Conversely, if the subject failed, the SSD decreased by one step.

Behavioural considerations

The countermanding task makes possible to calculate a behavioural measure that it is broadly considered as an index of efficiency in movement suppression: the Stop signal reaction time or SSRT. To estimate the SSRT the race model[73] is the accepted paradigm. This model describes the behaviour in the Stop trials as the result of two stochastic processes racing toward a threshold: the GO process triggered by the onset of the Go signal, which duration is represented by the RT, and the STOP process triggered by the onset of the Stop signal, which duration must be calculated. When the GO process wins the race the movement is generated (wrong Stop trials), alternatively it is withheld (correct Stop trials). The race model allows to estimate the SSRT by considering the duration of the GO process, the probability to respond, and the SSDs. However, to make the race model applicable to study response inhibition, a central assumption must be satisfied: the GO process in the Stop trials must be the same as in the Go trials (independence assumption). Indeed, the RTs that are employed to estimate the SSRT are obtained from the Go trials distributions. To broadly validate this assumption, wrong Stop trials RTs must result shorter than the correct Go trials RT[73] (see Table 1). To estimate the SSRT we employed the integration method because it has been proven to be the most reliable[74]. The method assumes that the finishing time of the Stop process corresponds to the *n*th Go RT, where *n* results from the multiplication of the ordered Go RTs distribution by the overall probability of responding $p(respond)$. The SSRT is then obtained by subtracting the average SSD from the *n*th Go RT. The SSRT can also be considered as the lead time that is required to inhibit a movement, or, simply, the time that precedes the start of a movement when a Stop signal, if presented, halts the generation of the same movement approximately 50% of the time. If the Stop signal is presented after this time, it will be less effective, because the neuronal phenomena that lead to the movement generation will have already started. If the Stop signal is presented well before this time, it will be more effective in halting the movement. Consequently, the neuronal activity that is related to movement generation must occur before movement onset around the time that is defined by the SSRT.

The aim of our study was to compare conditions in which a movement was planned and then generated (Go trials) to those in which a movement was planned and then inhibited (correct Stop trials). To correctly compare the two behavioural conditions, a time window (T) equivalent for both trial types must be defined. The duration of T corresponded to 400 ms. For Go trials, T was the last portion of the RT. For Stop trials, T allowed to include any SSRT duration computed in the different sessions (see Table 1) and a variable

bioRxiv preprint doi: https://doi.org/10.1101/2021.03.15.435381; this version posted May 10, 2021. The copyright holder for this preprint (which was not certified by peer review) is the author/funder, who has granted bioRxiv a license to display the preprint in perpetuity. It is made available under aCC-BY-NC-ND 4.0 International license.

portion of the SSD (controlling for the duration of the shortest used).

Behavioural parameters for the recording sessions of the two monkeys analyzed in this study are reported in Table 1.

Extraction and processing of neuronal data

A multielectrode array (Blackrock Microsystems, Salt Lake City) with 96 electrodes (spacing 0.4 mm) was surgically implanted in the left dorsal premotor cortex (PMd; arcuate sulcus and pre-central dimple used as references after opening of the dura) to acquire unfiltered electric field potentials (UFP; i.e., the raw signal), sampled at 24.4 kHz (Tucker Davis Technologies, Alachua, FL). As a measure of neuronal activity at the population level, SA was extracted offline from the raw signal, as in Mattia et al.[7], by computing the time-varying power spectra P(ω, t) from the short-time Fourier transform of the signal in 5-ms sliding windows. Relative spectra R(ω, t) were then obtained normalizing P(ω, t) by their average P_{ref} (ω) across a fixed window (30 minutes) for the entire recording. Thus, the average R(ω, t) across the $\omega/2\pi$ band $[0.2, 1.5]$ kHz represent the spectral estimated SAs. As better detailed in Mattia et al.[7], such estimate relies on two hypotheses. The first is that high ω components of the raw signal result from the convolution of firing rates ν(t) of neurons that are close to the electrode tip with a stereotypical single-unit waveform. The Fourier transform K(ω) of such an unknown waveform is canceled out in R(ω, t), which is therefore a good approximation of the ratio of firing rate spectra $|\nu(\omega,t)|^2 / |\nu(\omega,t)|_{ref}{}^2$. The second hypothesis is that high ω power $|\nu(\omega,t)|^2$ is proportional to the firing rate ν(t) itself[75], such that our SA estimate is proportional to ν(t). As a last step, logarithmically scaled SAs were smoothed by a moving average (20 ms sliding window, 5ms step).

Quantifying information dynamics with Transfer Entropy

We first analysed the single-trials activity profiles of each recording site of each recording session for both animals. To remove noise and outliers from our data, we excluded from the analysis the trials for which the SA showed peaks with an amplitude that exceeded the average of the activity by 2 standard deviations in the epoch of interest and for over 80% of the channels. This ensures that artifacts caused by non-physiological oscillations are excluded from the analysis. To examine the local information dynamics in the PMd, we then computed a trial-average time series for each of the SAs recorded by the electrodes of the array for each behavioural condition of each recording session. We then constructed the information transfer network using multivariate Transfer Entropy (*TE*). The choice is due to the fact that TE is indicated (especially in its multivariate formulations) as more accurate compared to other metrics and is known to capture non-linear interaction in the system dynamic without assuming any particular model. Moreover, this measure is of growing interest in neuroscience and there is a thriving literature on it[76–80]. For its computation we used the Matlab *MUTE* toolbox[81].

Given an ensemble of M time series, the multivariate information transfer from a *driver* time series X to a *target* time series Y, conditioned to the remaining $Z_{k=1,..,M-2}$ time series, can be quantified taking into account the present values of the target and the past values of both the driver and the Z[76,81,82] through:

$$TE_{X\to Y\,|\,Z} = H(Y_n \mid Y_n^-, Z_n^-) - H(Y_n \mid X_n^-, Y_n^-, Z_n^-)\,, \tag{1}$$

where Y_n is the vector that represent the present state n of Y, $X_n^- = [X_{n-1}, X_{n-2}, ...]$, $Y_n^- = [Y_{n-1}, Y_{n-2}, ...]$ and $Z_n^- = [Z_{n-1}, Z_{n-2}, ...]$ are the vectors that represent the past of X, Y and Z respectively. The vertical bar stands for conditional probability, e.g. $H(Y_n \mid Y_n^-, Z_n^-)$ is the entropy of the present state of Y conditioned to the knowledge of the past of Y and to the past of the remaining Z. H is the Shannon entropy[83], which in the case of Y is given by:

$$H(Y_n) = -\sum_n P(Y_n)\, log P(Y_n)\,, \tag{2}$$

bioRxiv preprint doi: https://doi.org/10.1101/2021.03.15.435381; this version posted May 10, 2021. The copyright holder for this preprint (which was not certified by peer review) is the author/funder, who has granted bioRxiv a license to display the preprint in perpetuity. It is made available under aCC-BY-NC-ND 4.0 International license.

where P indicates the probability density. Hence, using equation 2 expression 1 becomes

$$TE_{X\rightarrow Y\mid Z} = -\sum_{n} P(Y_n, Y_n^-, Z_n^-)\; log\frac{P(Y_n \mid X_n^-, Y_n^-, Z_n^-)}{P(Y_n \mid Y_n^-, Z_n^-)} \tag{3}$$

In this formulation *TE* grows if the past of the driver increases the information about the present of target more than the past of target itself and more than any other series contained in Z. Since the past of the driver is used to predict the present of the target, TE is not symmetric (i.e. $TE_{X\rightarrow Y} \neq TE_{Y\rightarrow X}$) and defines a direction in the information transfer. A crucial issue when estimating TE is the approximation of the vectors representing the past of the time series, a procedure known as *embedding*. The optimal embedding would be the one that includes only the components of X_n^-, Y_n^- and Z_n^- that are most informative in describing Y_n. Montalto et al.[81] described in details different procedures both for embedding and to evaluate the probability distribution functions needed to compute the entropy terms. We opted for a non-uniform embedding scheme[84] paired with the computation of H based on kernels estimators[1]. In few words, the embedding method we chose iteratively selects components of the systems past based on a criterion for maximum relevance and minimum redundancy. In this context, maximum relevance means most significant in the sense of predictive information. Non-uniform embedding selects from the past of X, Y and Z only the components that are the most informative for the present of the target variable Y, progressively pruning non informative terms. The maximum number of past values, or maximum lag l, to consider for the pruning is fixed at the beginning of the procedure. The statistical significance is then progressively assessed cycling through the components of the past up to l and through the comparison with an null distribution built from the empirical values via a randomization procedure[81]. The component of the past of X,Y and Z are thus selected as statistical significant if they are significant above a desired level α. In our case the null distribution was obtained by 100 random shuffling of empirical values and we fixed $\alpha = 0.01$. Non-uniform embedding represents a convenient and more reliable[76] alternative to the common used approach known as uniform embedding that would select the past values X_n^-, Y_n^- and Z_n^- *a priori* and separately for each time series[81]. The probability density P needed for the computations of H was then calculated using kernel functions which weight the distance to the reference point to any other point in the time series and then average across all points. Such approach computes probabilities exploiting a local exploring of the state space and, importantly, has been proven to be more robust against unreliable estimations compared to other approaches[76]. Therefore, if at least one component from the past is selected by the non-uniform embedding procedure, the resulting $TE_{X\rightarrow Y\mid Z}$ is positive and statistically significant. When instead none of the components of the past provide statically significant information about the target the $TE_{X\rightarrow Y\mid Z}$ is exactly 0 and assumed non significant[81]. To avoid any further bias in the selection of the past values, we initially fixed l=50 ms, but, as expected, only a recent past was selected by the procedure, in line with similar studies[26,31]. Indeed, for each SA time series, a past no older than 10ms for each n of equation 2 was ever selected by the optimal embedding procedure.

Graph theoretical measures

In our context the time series were the SAs recorded by the electrodes of the array. We computed $TE_{X\rightarrow Y\mid Z}$ (and $TE_{Y\rightarrow X\mid Z}$) with $Z_{k=1,..,M-2}$, for each pair of (X,Y) in the epochs defined in Section 1 so to obtain a TE matrix[2] for each behavioural condition (Go trials and correct Stop trials) for both

[1] For the complete description of the embedding methods and estimators for computation of H, which is beyond the scope of this study, see the works of Faes and colleagues[82,84,85] and references therein.

[2] 96x96 for all recording sessions for Monkey P; for some recording sessions of Monkey C damaged channels were removed from the analysis and therefore a 79x79 matrix was obtained.

bioRxiv preprint doi: https://doi.org/10.1101/2021.03.15.435381; this version posted May 10, 2021. The copyright holder for this preprint (which was not certified by peer review) is the author/funder, who has granted bioRxiv a license to display the preprint in perpetuity. It is made available under aCC-BY-NC-ND 4.0 International license.

monkeys. Since the purpose of this study was to investigate the topology of information processing within the PMd cortical network during motor planning and inhibition, we interpreted the asymmetric *TE* matrix as the adjacency matrix of a directed weighted network, in which the nodes are the single modules (electrodes) and the weighted edges are the $TE_{X \to Y \mid Z}$ (and $TE_{Y \to X \mid Z}$) with $Z_{k=1,..,M-2}$. To simplify the picture we considered only the off-diagonal elements of the matrix thus excluding self-loops from the networks. As an initial skimming of the contribution of each module to the exchange of information in the network we analyzed the empirical TE distributions. We grouped modules according to the trial type in which they significantly exchanged information with respect to the others. To this end we selected from the empirical TE distribution the values $> \mu + 2\sigma$ for each behavioural condition (with μ mean and σ standard deviation). The choice was justified by the observation of an high positive skewness (indicating a long right tail) and a $\mu \sim 10^{-}2$ for the TE distributions for all recording sessions of both behavioural conditions for both animals. This selection procedure identified the classes. For example, if node *i* drives node *j* with a TE value $> \mu + 2\sigma$ (i.e. there is a strong link directed from *i* to *j*) in Go trials but not in correct Stop trials, *i* would belong to the Go_drivers. In our framework, the TE values represented the strength of the connections between network nodes and hence the above classes are defined based of how much and during which behavioural condition nodes spread information trough the local PMd network.

To properly inspect the contribution of each node we needed a set of measures from graph theory. The first was Vertex Degree (VD). VD is the number of links to a node *i*:

$$VD(i) = \sum_{j=1}^{N} a_{ij} \ , \tag{4}$$

where a_{ij} is the generic entry of the adjacency matrix and N is the number of nodes. In directed networks one can distinguish between in-degree (the number on inward links) and out-degree (the number of outward links). We computed the probability distribution of both VDs (i.e. the in/out degree distribution) for each behavioural condition of each recording sessions for both animals. If the variance of the degree distribution is significantly larger than its mean, tails in the distribution arise and network hubs are identified (see Figure S1). Hubs are thus nodes that significantly exceed the average degree of the network[23]. We further studied the topology of the PMd information network by computing the Betweenness Centrality[24,25] (BC) of each node. For each node, BC measure the proportion of shortest paths between other couple of nodes *s* and *t* that pass through it and is defined as[24]:

$$BC(i) = \sum_{s \neq v \neq t} \frac{\sigma_{st}(i)}{\sigma_{st}} \ , \tag{5}$$

, where $\sigma_{st}(i)$ is the number of shortest paths between *s* and *t* that pass through *i* and σ_{st} the the number of shortest paths between *s* and *t*. High BC scores indicate that a node lies on a considerable fraction of shortest paths connecting pairs of vertices in the graph. Thus, such a node is considered a topological central node since it plays a crucial role in passing and spreading information through the network. In this study we used a normalized version of BC by dividing expression 5 by the normalization factor for directed graph $(N-1)(N-2)$ which takes into account the number of ordered pairs of nodes used for calculation (with N number of nodes). Then, for each recording sessions, we further scaled the so obtained BC value by its maximum value across behavioural conditions so that BC spanned the [0,1] interval.
As an overall measure of network comparison we used the centralization index *C*. Given a graph measure,

bioRxiv preprint doi: https://doi.org/10.1101/2021.03.15.435381; this version posted May 10, 2021. The copyright holder for this preprint (which was not certified by peer review) is the author/funder, who has granted bioRxiv a license to display the preprint in perpetuity. It is made available under aCC-BY-NC-ND 4.0 International license.

C is the total average difference between the maximum of that measure and the values taken by all other nodes in the network. i.e., C of VD_{out} reads:

$$C_{vd} = \frac{1}{N-1}\sum_{i=1}^{N}[Max(VD_{out}) - VD_{\text{out}}{}^{i}] \ , \tag{6}$$

where VD^{i}_{out} is the vertex out degree of node i, $Max(VD_{out})$ is the maximum VD_{out} value for the examined graph and N is the number of nodes. The same holds for BC. We computed C for both VD^{i}_{out} and BC for each recording session and each behavioural condition for both animals and then averaged over sessions. Finally, in order to compute the total magnitude of information exchanged between the neuronal classes we constructed the following interaction measure I:

$$I_{\text{ij}} = \rho \sum_{i}^{M}\sum_{j}^{M}\sum_{(m,n)} TE_{C_{\text{i}}{}^{\text{n}} \to C_{\text{j}}{}^{\text{n}}} \ , \tag{7}$$

where C is the module's class, M is the number of the classes (M=4) and m and n run over the all possible combinations of nodes within each class. $\rho = \frac{dim\,(C_{\text{i}}{}^{\text{n}} \to C_{\text{j}}{}^{\text{m}})}{dim\,(C_{\text{j}})}$ is a normalization factor that accounts for the heterogeneous number of nodes within each of the classes. Therefore, our I_{ij} is a normalized node strength computed on the graph formed by the 4 classes (i.e. in a weighted graph the strength of a node is the sum of the weights of the links connected to the node). The higher are the number of nodes a class transmits information to, the higher is I. Hence, the values and the directions of I values reflect the position in the hierarchy of the network communications for that class. All the interactions described by the empirical TE matrix were thus enclosed in a 4x4 matrix that represents a network of interactions in which now each node is a neuronal class. We computed I for each recording session and each behavioural condition and then we averaged over sessions for both animals. The uncertainty in estimating each element I_{ij} for each recording session was given by the standard error. Then, the sessions-averaged element $\bar{I}_{\text{ij}}$ (Figure 6 and Table 4) is estimated with an error obtained via the error propagation formula for the average of n measures.

A null model

To properly assess the statistical significance of the results obtained via the graph theoretical analysis we defined a null model. As extensively detailed in a recent work[86], the choice of a suitable null model remains a thorny issue in network and complex systems science. One common practice when analysing real-world networks such the one inspected in the present work, is try to identify properties that deviate from the null hypothesis, being likely that the deviations themselves encode information about the network functions. In this study, we drew our conclusions about the PMd information network in a completely data-driven fashion directly from neural activity, which thus constituted our only constraint. Therefore, we tested whether the results were not attributable to the distribution of SA values. To this end we generated, for each behavioural condition and recording session, a synthetic pool of N time series with same length of the empirical ones (with N number of channels available for the corresponding animal and recording session) by random sampling from the empirical SA distribution. We then computed the TE matrix for each synthetic pool. This situation is the most general since assumptions of any kind are made on the connectivity patterns and the weight distributions of the synthetic networks. We then compared the empirical graph measures with the ones obtained on the ensemble of 500 randomizations. To correctly compare the empirical graph measures (the out degree VD_{out} and betweenness centrality BC) with the ones

bioRxiv preprint doi: https://doi.org/10.1101/2021.03.15.435381; this version posted May 10, 2021. The copyright holder for this preprint (which was not certified by peer review) is the author/funder, who has granted bioRxiv a license to display the preprint in perpetuity. It is made available under aCC-BY-NC-ND 4.0 International license.

obtained on the ensemble of randomizations we computed the expected degree of the largest node in the randomized networks, also known as the *upper natural cutoff*[87]. This is defined as the degree for which the area under the degree distribution equals $\frac{1}{N}$ with N number of nodes (the same holds for the expected smallest degree). We computed the upper natural cutoff for the out degree, VD_{out}^{max} for each randomized network, obtaining a null distribution for each behavioural condition and each recording sessions of both monkeys with which to compare the corresponding empirical values (figure S4). Analogously, we computed the expected maximum *BC* of the ensemble of randomizations (figure S5).

VD_{Out}			
Monkey P			
Go trials	Go_drivers	Stop_drivers	Targets
Common_drivers	$Q < 0.005$	$Q < 0.001$	$Q < 0.001$
Stop trials	Go_drivers	Stop_drivers	Targets
Common_drivers	$Q < 0.001$	$Q < 0.01$	$Q < 0.001$
$\Delta_{Stop-Go}$			
Go_drivers	Stop_drivers	Common_drivers	Targets
-98% $Q < 0.001$	$+1370\%$ $Q < 0.001$	-18% $Q > 0.25$	-4% $Q > 0.25$
Monkey C			
Go trials	Go_drivers	Stop_drivers	Targets
Common_drivers	$Q < 0.01$	$Q < 0.001$	$Q < 0.001$
Stop trials	Go_drivers	Stop_drivers	Targets
Common_drivers	$Q < 0.001$	$Q < 0.01$	$Q < 0.001$
$\Delta_{Stop-Go}$			
Go_drivers	Stop_drivers	Common_drivers	Targets
-97% $Q < 0.001$	$+9828\%$ $Q < 0.001$	-29% $Q > 0.25$	-950% $Q > 0.25$

bioRxiv preprint doi: https://doi.org/10.1101/2021.03.15.435381; this version posted May 10, 2021. The copyright holder for this preprint (which was not certified by peer review) is the author/funder, who has granted bioRxiv a license to display the preprint in perpetuity. It is made available under aCC-BY-NC-ND 4.0 International license.

BC			
Monkey P			
Go trials	Go_drivers	Stop_drivers	Targets
Common_drivers	$Q > 0.05$	$Q < 0.001$	$Q < 0.001$
Stop trials	Go_drivers	Stop_drivers	Targets
Common_drivers	$Q < 0.001$	$Q < 0.001$	$Q < 0.001$
$\Delta_{Stop-Go}$			
Go_drivers	Stop_drivers	Common_drivers	Targets
-89% $Q < 0.001$	$+888\%$ $Q < 0.001$	$+157\%$ $Q < 0.001$	$+183\%$ $Q < 0.001$
Monkey C			
Go trials	Go_drivers	Stop_drivers	Targets
Common_drivers	$Q < 0.001$	$Q < 0.001$	$Q < 0.001$
Stop trials	Go_drivers	Stop_drivers	Targets
Common_drivers	$Q < 0.001$	$Q > 0.05$	$Q < 0.001$
$\Delta_{Stop-Go}$			
Go_drivers	Stop_drivers	Common_drivers	Targets
-95% $Q < 0.001$	$+5180\%$ $Q < 0.001$	$+654\%$ $Q < 0.001$	$+800\%$ $Q > 0.25$

Table 3. Graph metrics details.

bioRxiv preprint doi: https://doi.org/10.1101/2021.03.15.435381; this version posted May 10, 2021. The copyright holder for this preprint (which was not certified by peer review) is the author/funder, who has granted bioRxiv a license to display the preprint in perpetuity. It is made available under aCC-BY-NC-ND 4.0 International license.

***I* matrix details**				
Monkey P				
Go trials	Go_drivers	Stop_drivers	Common_drivers	Targets
Go_drivers	0	1.3 ± 0.1	0	17.5 ± 0.3
Stop_drivers	0	0	0	0
Common_drivers	3.7 ± 0.1	7 ± 0.2	0	42.3 ± 0.4
Targets	0	0	0	0
Stop trials	Go_drivers	Stop_drivers	Common_drivers	Targets
Go_drivers	0	0	0	0
Stop_drivers	2.6 ± 0.2	0	0	17.5 ± 0.6
Common_drivers	2.3 ± 0.2	4.7 ± 0.4	0	25.4 ± 0.6
Targets	0	0	0	0
Monkey C				
Go trials	Go_drivers	Stop_drivers	Common_drivers	Targets
Go_drivers	0	1.1 ± 0.1	0.3 ± 0.003	21 ± 0.5
Stop_drivers	0	0	0	0
Common_drivers	3.4 ± 0.07	10.7 ± 0.2	0	45.3 ± 0.6
Targets	0	0	0	0
Stop trials	Go_drivers	Stop_drivers	Common_drivers	Targets
Go_drivers	0	0	0	0
Stop_drivers	1.9 ± 0.2	0	0	17 ± 0.6
Common_drivers	2.9 ± 0.2	1.4 ± 0.2	0	23.4 ± 0.5
Targets	0	0	0	0

Table 4. *I* matrix details.

bioRxiv preprint doi: https://doi.org/10.1101/2021.03.15.435381; this version posted May 10, 2021. The copyright holder for this preprint (which was not certified by peer review) is the author/funder, who has granted bioRxiv a license to display the preprint in perpetuity. It is made available under aCC-BY-NC-ND 4.0 International license.

Acknowledgements

Partially supported by grants from Sapienza University and EU FP7 grant 'BrainLeap'

Author contributions statement

F.G, P.P., E.B. and S.F conceived the experiment, F.G. and P.P. conducted the experiment, G.B. analysed the results. All authors reviewed the manuscript.

Competing interests

(mandatory statement)

None.

bioRxiv preprint doi: https://doi.org/10.1101/2021.03.15.435381; this version posted May 10, 2021. The copyright holder for this preprint (which was not certified by peer review) is the author/funder, who has granted bioRxiv a license to display the preprint in perpetuity. It is made available under aCC-BY-NC-ND 4.0 International license.

References

1. Hong, G. & Lieber, C. M. Novel electrode technologies for neural recordings. *Nat. Rev. Neurosci.* **20**, 330–345, 10.1038/s41583-019-0140-6 (2019).

2. Ferraina, S. & Pare, M. Comparison of Cortico-Cortical and Cortico-Collicular Signals for the Generation of Saccadic Eye Movements Working memory storage limitations View project Executive control and decision making View project. *Article J. Neurophysiol.* 10.1152/jn.00317.2001 (2002).

3. Wurtz, R. H., Sommer, M. A., Paré, M. & Ferraina, S. Signal transformations from cerebral cortex to superior colliculus for the generation of saccades. *Vis. Res.* **41**, 3399–3412, 10.1016/S0042-6989(01)00066-9 (2001).

4. Herreras, O. Local Field Potentials: Myths and Misunderstandings. *Front. Neural Circuits* **10**, 101, 10.3389/fncir.2016.00101 (2016).

5. Stark, E. & Abeles, M. Predicting movement from multiunit activity. *J. Neurosci.* **27**, 8387–8394, 10.1523/JNEUROSCI.1321-07.2007 (2007).

6. Trautmann, E. M. *et al.* Accurate Estimation of Neural Population Dynamics without Spike Sorting. *Neuron* **103**, 292–308, 10.1016/j.neuron.2019.05.003 (2019).

7. Mattia, M. *et al.* Heterogeneous attractor cell assemblies for motor planning in premotor cortex. *J. Neurosci.* **33**, 11155–11168, 10.1523/JNEUROSCI.4664-12.2013 (2013).

8. Wise, S. P., Boussaoud, D., Johnson, P. B. & Caminiti, R. Premotor and parietal cortex: Corticocortical connectivity and combinatorial computations, 10.1146/annurev.neuro.20.1.25 (1997).

9. Cisek, P. & Kalaska, J. F. Neural mechanisms for interacting with a world full of action choices, 10.1146/annurev.neuro.051508.135409 (2010).

10. Shenoy, K. V., Sahani, M. & Churchland, M. M. Cortical Control of Arm Movements: A Dynamical Systems Perspective. *Annu. Rev. Neurosci.* **36**, 337–359, 10.1146/annurev-neuro-062111-150509 (2013).

11. Riehle, A., Grün, S., Diesmann, M. & Aertsen, A. Spike synchronization and rate modulation differentially involved in motor cortical function. *Science* **278**, 1950–1953, 10.1126/science.278.5345.1950 (1997).

12. Georgopoulos, A. P., Schwartz, A. B. & Kettner, R. E. Neuronal population coding of movement direction. *Science* **233**, 1416–1419, 10.1126/science.3749885 (1986).

13. Munoz, D. P. & Wurtz, R. H. Fixation cells in monkey superior colliculus I. Characteristics of cell discharge. *J. Neurophysiol.* **70**, 559–575, 10.1152/jn.1993.70.2.559 (1993).

14. Schall, J. D. Visuomotor Functions in the Frontal Lobe. *Annu. Rev. Vis. Sci.* **1**, 469–498, 10.1146/annurev-vision-082114-035317 (2015).

15. Vaadia, E., Kurata, K. & Wise, S. P. Neuronal activity preceding directional and nondirectional cues in the premotor cortex of rhesus monkeys. *Somatosens. & Mot. Res.* **6**, 207–230, 10.3109/08990228809144674 (1988).

16. Fetz, E. E. Are movement parameters recognizably coded in the activity of single neurons? *Behav. Brain Sci.* **15**, 679–690, 10.1017/S0140525X00072599 (1992).

17. Vyas, S., Golub, M. D., Sussillo, D. & Shenoy, K. V. Computation through Neural Population Dynamics, 10.1146/annurev-neuro-092619-094115 (2020).

bioRxiv preprint doi: https://doi.org/10.1101/2021.03.15.435381; this version posted May 10, 2021. The copyright holder for this preprint (which was not certified by peer review) is the author/funder, who has granted bioRxiv a license to display the preprint in perpetuity. It is made available under aCC-BY-NC-ND 4.0 International license.

18. Bardella, G., Pani, P., Brunamonti, E., Giarrocco, F. & Ferraina, S. The small scale functional topology of movement control: Hierarchical organization of local activity anticipates movement generation in the premotor cortex of primates. *NeuroImage* **207**, 10.1016/j.neuroimage.2019.116354 (2020).

19. Giarrocco, F. *et al.* Neuronal dynamics of signal selective motor plan cancellation in the macaque dorsal premotor cortex. *Cortex* **135**, 326–340, 10.1016/j.cortex.2020.09.032 (2021).

20. Hubel, D. H. & Wiesel, T. N. Receptive fields, binocular interaction and functional architecture in the cat's visual cortex. *The J. Physiol.* **160**, 106–154, 10.1113/jphysiol.1962.sp006837 (1962).

21. Stuphorn, V. Neural mechanisms of response inhibition, 10.1016/j.cobeha.2014.10.009 (2015).

22. Schreiber, T. Measuring information transfer. *Phys. Rev. Lett.* **85**, 461–464, 10.1103/PhysRevLett.85.461 (2000).

23. Albert, R. & Barabási, A.-L. Statistical mechanics of complex networks. *Rev. Mod. Phys.* **74**, 47–97, 10.1103/RevModPhys.74.47 (2002).

24. Freeman, L. C. A Set of Measures of Centrality Based on Betweenness. *Sociometry* **40**, 35, 10.2307/3033543 (1977).

25. White, D. R. & Borgatti, S. P. Betweenness centrality measures for directed graphs. Tech. Rep. (1994).

26. Shimono, M. & Beggs, J. M. Functional clusters, hubs, and communities in the cortical microconnectome. *Cereb. Cortex* **25**, 3743–3757, 10.1093/cercor/bhu252 (2015).

27. Buehlmann, A. & Deco, G. Optimal information transfer in the cortex through synchronization. *PLoS Comput. Biol.* **6**, 1000934, 10.1371/journal.pcbi.1000934 (2010).

28. Orlandi, J. G., Stetter, O., Soriano, J., Geisel, T. & Battaglia, D. Transfer entropy reconstruction and labeling of neuronal connections from simulated calcium imaging. *PLoS ONE* **9**, 98842, 10.1371/journal.pone.0098842 (2014).

29. Ito, S. *et al.* Extending Transfer Entropy Improves Identification of Effective Connectivity in a Spiking Cortical Network Model. *PLoS ONE* **6**, e27431, 10.1371/journal.pone.0027431 (2011).

30. Nigam, S. *et al.* Rich-club organization in effective connectivity among cortical neurons. *J. Neurosci.* **36**, 655–669, 10.1523/JNEUROSCI.2177-15.2016 (2016).

31. Timme, N. M. *et al.* High-Degree Neurons Feed Cortical Computations. *PLOS Comput. Biol.* **12**, e1004858, 10.1371/journal.pcbi.1004858 (2016).

32. Gerhard, F., Pipa, G., Lima, B., Neuenschwander, S. & Gerstner, W. Extraction of Network Topology From Multi-Electrode Recordings: Is there a Small-World Effect? *Front. Comput. Neurosci.* **5**, 4, 10.3389/fncom.2011.00004 (2011).

33. Besserve, M., Lowe, S. C., Logothetis, N. K., Schölkopf, B. & Panzeri, S. Shifts of Gamma Phase across Primary Visual Cortical Sites Reflect Dynamic Stimulus-Modulated Information Transfer. *PLoS Biol.* **13**, e1002257, 10.1371/journal.pbio.1002257 (2015).

34. Honey, C. J., Kötter, R., Breakspear, M. & Sporns, O. Network structure of cerebral cortex shapes functional connectivity on multiple time scales. *Proc. Natl. Acad. Sci. United States Am.* **104**, 10240–10245, 10.1073/pnas.0701519104 (2007).

35. Jahfari, S. *et al.* Effective connectivity reveals important roles for both the hyperdirect (fronto-subthalamic) and the indirect (fronto-striatal-pallidal) fronto-basal ganglia pathways during response inhibition. *J. Neurosci.* **31**, 6891–6899, 10.1523/JNEUROSCI.5253-10.2011 (2011).

bioRxiv preprint doi: https://doi.org/10.1101/2021.03.15.435381; this version posted May 10, 2021. The copyright holder for this preprint (which was not certified by peer review) is the author/funder, who has granted bioRxiv a license to display the preprint in perpetuity. It is made available under aCC-BY-NC-ND 4.0 International license.

36. Boucher, L., Palmeri, T. J., Logan, G. D. & Schall, J. D. Inhibitory control in mind and brain: An interactive race model of countermanding saccades. *Psychol. Rev.* **114**, 376–397, 10.1037/0033-295X.114.2.376 (2007).

37. Lo, C. C., Boucher, L., Paré, M., Schall, J. D. & Wang, X. J. Proactive inhibitory control and attractor dynamics in countermanding action: A spiking neural circuit model. *J. Neurosci.* **29**, 9059–9071, 10.1523/JNEUROSCI.6164-08.2009 (2009).

38. Churchland, M. M. *et al.* Neural population dynamics during reaching. *Nature* **487**, 51–56, 10.1038/nature11129 (2012).

39. Chandrasekaran, C., Peixoto, D., Newsome, W. T. & Shenoy, K. V. Laminar differences in decision-related neural activity in dorsal premotor cortex. *Nat. Commun.* **8**, 1–16, 10.1038/s41467-017-00715-0 (2017).

40. Kaufman, M. T. *et al.* The largest response component in the motor cortex reflects movement timing but not movement type. *eNeuro* **3**, 85–101, 10.1523/ENEURO.0085-16.2016 (2016).

41. Clawson, W. *et al.* Computing hubs in the hippocampus and cortex. *Sci. Adv.* **5**, eaax4843, 10.1126/sciadv.aax4843 (2019).

42. Schroeder, K. E. *et al.* Disruption of corticocortical information transfer during ketamine anesthesia in the primate brain. *NeuroImage* **134**, 459–465, 10.1016/j.neuroimage.2016.04.039 (2016).

43. Marcos, E. *et al.* Neural variability in premotor cortex is modulated by trial history and predicts behavioral performance. *Neuron* **78**, 249–255, 10.1016/j.neuron.2013.02.006 (2013).

44. Verbruggen, F. & Logan, G. D. Response inhibition in the stop-signal paradigm, 10.1016/j.tics.2008.07.005 (2008).

45. Schall, J. D., Palmeri, T. J. & Logan, G. D. Models of inhibitory control. *Philos. Transactions Royal Soc. B: Biol. Sci.* **372**, 20160193, 10.1098/rstb.2016.0193 (2017).

46. Wei, W., Rubin, J. E. & Wang, X. J. Role of the indirect pathway of the basal ganglia in perceptual decision making. *J. Neurosci.* **35**, 4052–4064, 10.1523/JNEUROSCI.3611-14.2015 (2015).

47. Gu, Y., Qi, Y. & Gong, P. Rich-club connectivity, diverse population coupling, and dynamical activity patterns emerging from local cortical circuits. *PLoS Comput. Biol.* **15**, e1006902, 10.1371/journal.pcbi.1006902 (2019).

48. Perin, R., Berger, T. K. & Markram, H. A synaptic organizing principle for cortical neuronal groups. *Proc. Natl. Acad. Sci. United States Am.* **108**, 5419–5424, 10.1073/pnas.1016051108 (2011).

49. Timme, N. *et al.* Multiplex Networks of Cortical and Hippocampal Neurons Revealed at Different Timescales. *PLoS ONE* **9**, e115764, 10.1371/journal.pone.0115764 (2014).

50. Schroeter, M. S., Charlesworth, P., Kitzbichler, M. G., Paulsen, O. & Bullmore, E. T. Emergence of rich-club topology and coordinated dynamics in development of hippocampal functional networks In vitro. *J. Neurosci.* **35**, 5459–5470, 10.1523/JNEUROSCI.4259-14.2015 (2015).

51. Gal, E. *et al.* Rich cell-type-specific network topology in neocortical microcircuitry. *Nat. Neurosci.* **20**, 1004–1013, 10.1038/nn.4576 (2017).

52. Dann, B., Michaels, J. A., Schaffelhofer, S. & Scherberger, H. Uniting functional network topology and oscillations in the fronto-parietal single unit network of behaving primates. *eLife* **5**, 10.7554/eLife.15719 (2016).

bioRxiv preprint doi: https://doi.org/10.1101/2021.03.15.435381; this version posted May 10, 2021. The copyright holder for this preprint (which was not certified by peer review) is the author/funder, who has granted bioRxiv a license to display the preprint in perpetuity. It is made available under aCC-BY-NC-ND 4.0 International license.

53. Hilgetag, C., O'Neill, M. A. & Young, M. P. Hierarchical organization of macaque and cat cortical sensory systems explored with a novel network processor. *Philos. Transactions Royal Soc. London. Ser. B: Biol. Sci.* **355**, 71–89, 10.1098/rstb.2000.0550 (2000).

54. Hilgetag, C. C. & Kaiser, M. Clustered organization of cortical connectivity, 10.1385/NI:2:3:353 (2004).

55. Felleman, D. J., Felleman, D. J. & Van Essen, D. C. Distributed hierarchical processing in the primate cerebral cortex. *CEREB CORTEX* 1–47 (1991).

56. Sporns, O., Tononi, G. & Kötter, R. The Human Connectome: A Structural Description of the Human Brain. *PLoS Comput. Biol.* **1**, e42, 10.1371/journal.pcbi.0010042 (2005).

57. Kaiser, M. Hierarchy and dynamics of neural networks. *Front. Neuroinformatics* **4**, 112, 10.3389/fninf.2010.00112 (2010).

58. Zamora-López. Cortical hubs form a module for multisensory integration on top of the hierarchy of cortical networks. *Front. Neuroinformatics* **4**, 1, 10.3389/neuro.11.001.2010 (2010).

59. Zeki, S. & Shipp, S. The functional logic of cortical connections, 10.1038/335311a0 (1988).

60. Tononi, G., Sporns, O. & Edelman, G. M. A measure for brain complexity: Relating functional segregation and integration in the nervous system. *Proc. Natl. Acad. Sci. United States Am.* **91**, 5033–5037, 10.1073/pnas.91.11.5033 (1994).

61. Sporns, O., Honey, C. J. & Kötter, R. Identification and Classification of Hubs in Brain Networks. *PLoS ONE* **2**, e1049, 10.1371/journal.pone.0001049 (2007).

62. Watanabe, T. *et al.* Energy landscapes of resting-state brain networks. *Front. Neuroinformatics* **8**, 12, 10.3389/fninf.2014.00012 (2014).

63. Kaiser, M., Görner, M. & Hilgetag, C. C. Criticality of spreading dynamics in hierarchical cluster networks without inhibition. *New J. Phys.* **9**, 110, 10.1088/1367-2630/9/5/110 (2007).

64. Bardella, G., Bifone, A., Gabrielli, A., Gozzi, A. & Squartini, T. Hierarchical organization of functional connectivity in the mouse brain: A complex network approach. *Sci. Reports* **6**, 1–11, 10.1038/srep32060 (2016).

65. Hilgetag, C. C. & Goulas, A. 'Hierarchy' in the organization of brain networks. *Philos. Transactions Royal Soc. B: Biol. Sci.* **375**, 20190319, 10.1098/rstb.2019.0319 (2020).

66. Fox, M. D. *et al.* The human brain is intrinsically organized into dynamic, anticorrelated functional networks. *Proc. Natl. Acad. Sci. United States Am.* **102**, 9673–9678, 10.1073/pnas.0504136102 (2005).

67. He, B. J. Scale-free properties of the functional magnetic resonance imaging signal during rest and task. *J. Neurosci.* **31**, 13786–13795, 10.1523/JNEUROSCI.2111-11.2011 (2011).

68. Zalesky, A., Fornito, A., Cocchi, L., Gollo, L. L. & Breakspear, M. Time-resolved resting-state brain networks. *Proc. Natl. Acad. Sci. United States Am.* **111**, 10341–10346, 10.1073/pnas.1400181111 (2014).

69. Shine, J. M. *et al.* The Dynamics of Functional Brain Networks: Integrated Network States during Cognitive Task Performance. *Neuron* **92**, 544–554, 10.1016/j.neuron.2016.09.018 (2016).

70. Vidaurre, D., Smith, S. M. & Woolrich, M. W. Brain network dynamics are hierarchically organized in time. *Proc. Natl. Acad. Sci. United States Am.* **114**, 12827–12832, 10.1073/pnas.1705120114 (2017).

bioRxiv preprint doi: https://doi.org/10.1101/2021.03.15.435381; this version posted May 10, 2021. The copyright holder for this preprint (which was not certified by peer review) is the author/funder, who has granted bioRxiv a license to display the preprint in perpetuity. It is made available under aCC-BY-NC-ND 4.0 International license.

71. Morcos, A. S. & Harvey, C. D. History-dependent variability in population dynamics during evidence accumulation in cortex. *Nat. Neurosci.* **19**, 1672–1681, 10.1038/nn.4403 (2016).

72. Mirabella, G., Pani, P. & Ferraina, S. Neural correlates of cognitive control of reaching movements in the dorsal premotor cortex of rhesus monkeys. *J. Neurophysiol.* **106**, 1454–1466, 10.1152/jn.00995.2010 (2011).

73. Logan, G. D. & Cowan, W. B. On the ability to inhibit thought and action: A theory of an act of control. *Psychol. Rev.* **91**, 295–327, 10.1037//0033-295x.91.3.295 (1984).

74. Band, G. P., van der Molen, M. W. & Logan, G. D. Horse-race model simulations of the stop-signal procedure. *Acta Psychol.* **112**, 105–142, 10.1016/S0001-6918(02)00079-3 (2003).

75. Mattia, M. & Del Giudice, P. Population dynamics of interacting spiking neurons. *Phys. Rev. E - Stat. Physics, Plasmas, Fluids, Relat. Interdiscip. Top.* **66**, 19, 10.1103/PhysRevE.66.051917 (2002).

76. Xiong, W., Faes, L. & Ivanov, P. C. Entropy measures, entropy estimators, and their performance in quantifying complex dynamics: Effects of artifacts, nonstationarity, and long-range correlations. *Phys. Rev. E* **95**, 1–37, 10.1103/PhysRevE.95.062114 (2017).

77. Wollstadt, P., Martínez-Zarzuela, M., Vicente, R., Díaz-Pernas, F. J. & Wibral, M. Efficient transfer entropy analysis of non-stationary neural time series. *PLoS ONE* **9**, 102833, 10.1371/journal.pone.0102833 (2014).

78. Vicente, R., Wibral, M., Lindner, M. & Pipa, G. Transfer entropy-a model-free measure of effective connectivity for the neurosciences. *J. Comput. Neurosci.* **30**, 45–67, 10.1007/s10827-010-0262-3 (2011).

79. Wibral, M. *et al.* Transfer entropy in magnetoencephalographic data: Quantifying information flow in cortical and cerebellar networks. *Prog. Biophys. Mol. Biol.* **105**, 80–97, 10.1016/j.pbiomolbio.2010.11.006 (2011).

80. Ramos, A. & Macau, E. Minimum Sample Size for Reliable Causal Inference Using Transfer Entropy. *Entropy* **19**, 150, 10.3390/e19040150 (2017).

81. Montalto, A., Faes, L. & Marinazzo, D. MuTE: A MATLAB toolbox to compare established and novel estimators of the multivariate transfer entropy. *PLoS ONE* **9**, e109462, 10.1371/journal.pone.0109462 (2014).

82. Faes, L., Kugiumtzis, D., Nollo, G., Jurysta, F. & Marinazzo, D. Estimating the decomposition of predictive information in multivariate systems. *PHYSICAL REVIEW E* **91**, 32904, 10.1103/PhysRevE.91.032904 (2015).

83. Shannon, C. E. A Mathematical Theory of Communication. Tech. Rep.

84. Faes, L., Marinazzo, D., Montalto, A. & Nollo, G. Lag-specific transfer entropy as a tool to assess cardiovascular and cardiorespiratory information transfer. *IEEE Transactions on Biomed. Eng.* **61**, 2556–2568, 10.1109/TBME.2014.2323131 (2014).

85. Faes, L., Nollo, G. & Porta, A. Information-based detection of nonlinear Granger causality in multivariate processes via a nonuniform embedding technique. *Phys. Rev. E - Stat. Nonlinear, Soft Matter Phys.* **83**, 051112, 10.1103/PhysRevE.83.051112 (2011).

86. Cimini, G. *et al.* The statistical physics of real-world networks. *Nat. Rev. Phys.* **1**, 58–71, 10.1038/s42254-018-0002-6 (2019).

87. Barabási, A. L. Network science, 10.1098/rsta.2012.0375 (2013).